Aerosol hygroscopicity and CCN activity during the AC^{3}Exp13 campaign: implications for CCN parameterization

F. Zhang[1]， Z. Li*[1,2], Y. N. Li[1], L. Sun[3], R.J. Li[1], C. Zhao[1], P. C. Wang[3], Y.L.Sun[3], X. G. Liu[4], J.X. Li[5,6], P. R. Li[5], G. Ren[5], T. Y. Fan[1]

[1]*College of Global Change and Earth System Science, Beijing Normal University, Beijing 100875, China*

[2]*Earth System Science Interdisciplinary Center and Department of Atmospheric and Oceanic Science, University of Maryland, College Park, Maryland, USA.*

[3]*State Key Laboratory of Atmospheric Boundary Layer Physics and Atmospheric Chemistry, Institute of Atmospheric Physics, Chinese Academy of Sciences, Beijing 100029, China*

[4]*State Key Laboratory of Water Environment Simulation, School of Environment, Beijing Normal University, Beijing 100875, China*

[5]*Weather Modification Office of Shanxi Province, Taiyuan, China, 030032*

[6]*Key Laboratory for Aerosol-Cloud-Precipitation of China Meteorological Administration , Nanjing University of Information Science and Technology, Nanjing,China,210044*

***correspondence to*: Z. Li (zli@atmos.umd.edu)**

Abstract

Aerosol hygroscopicity and cloud condensation nuclei (CCN) activity under background conditions and during polluted events are investigated during the Aerosol-CCN-Cloud Closure Experiment (AC^{3}Exp) campaign conducted at Xianghe, China in summer 2013. A gradual increase in activation ratio (AR) dependence on particle diameter (D_p) suggests that aerosol particles have lower hygroscopicity and heterogeneity of the composition during the campaign. Both activation diameter (D_a) and cut-off diameter (D_{cut}) were increased significantly at lower super saturations (SS) (<0.2%) due to pollutions (e.g. biomass burnings); the increase was not observed when SS>0.4%. Hygroscopicity parameter kappa (κ) are about 0.31-0.38 for particles in accumulation mode under background conditions and about 20% higher than that derived under polluted conditions; however, κ are about 0.20-0.34 for particles in nucleation or Aitken mode at background cases, showing slightly lower than that during polluted events. Larger particles were on average more hygroscopic than smaller particles. But the case is more complex for particles with heavy pollutions due to the diversities of particle compositions and mixing state. A non-parallel observation (NPO) CCN closure test shows about 30%-40% uncertainties in N_{CCN} prediction are associated with the changes of particle composition. A case study shows that CCN activation ratio increased with the increase of condensation nuclei (CN) number concentrations (N_{CN}) in background days. In the case, AR exhibited good correlation with κ_{chem}, which is calculated from chemical volume fractions. On the contrary, AR declined with increase of N_{CN} during polluted events, but it is closely related to *f*44,

which is usually associated with particle organic oxidation level. Our study highlights the importance of chemical composition on determining the particles activation properties, underlining the significance of long-term observation of CCN under different atmospheric environments, especially those regions with heavy pollutions.

1. Introduction

Indirect influence of aerosol particles on the radiative balance of the atmosphere through changes in cloud droplet number and persistence of clouds (Twomey, 1974; Albrecht, 1989), carries the largest uncertainty amongst the presently known causes of radiative forcing (IPCC, 2007, 2013). Thus, better understanding of aerosol formation, growth and activation is essential.

Field and laboratory experiments have been conducted with the aim of better characterizing the particle physical and chemical parameters impacting on cloud condensation nuclei (CCN) activation. Studies have addressed the relative importance of the size distribution, particle composition and mixing state in determining CCN activation, but there are disagreements on the relative importance of these parameters (e.g. Roberts et al., 2002; Feingold, 2003; Ervens et al., 2005; Mircea et al., 2005; Dusek et al., 2006a; Anttila and Kerminen, 2007; Hudson, 2007; Quinn et al., 2008; Zhang et al., 2008; Deng et al., 2013, Ma et al. 2013). CCN closure studies are a useful approach to test our knowledge of the controlling physical and chemical factors and help verify experimental results. CCN number concentration, N_{CCN}, is usually predicted from measured aerosol properties such as size distribution and composition or hygroscopicity based on Köhler theory. The closure between the measured and estimated N_{CCN} is often able to achieve in the background atmosphere without heavy pollutions (Chuang et al., 2000; Dusek et al., 2003;VanReken et al., 2003; Rissler et al., 2004; Gasparini et al.,2006; Stroud et al., 2007, Bougiatioti et al., 2009).

In urban/polluted areas, the particle size distribution is more complex with various composition of air mass (Lee et al., 2003; Alfarra et al., 2004; Zhang et al., 2004a; Salcedo et al., 2006). The particle activation is affected by composition and mixing state of the aerosol particles. It has been demonstrated that particles are more difficult

to be activated during biomass burning plumes (Mircea et al., 2005; Lee et al., 2006; Clarke et al., 2007; Rose et al., 2010, 2011; Paramonov et al., 2013; Lathem et al., 2013). Also, their activation ratios were reduced by secondary organics formed from oxidation of common biogenic emissions (VanReken et al., 2005; Varutbangkul et al., 2006; Mei et al., 2013) and black carbon (Dusek et al., 2006b; Kuwata et al., 2007). Other organic components (e.g. organic acids) are shown to activate more easily (Raymond and Pandis, 2002; Hartz et al., 2006; Bougiatioti et al., 2011), but still much less than inorganic species. Therefore, heavy polluted areas represent one of the most challenging cases to test the understanding of parameters controlling CCN activation and growth. Furthermore, the main uncertainty in predicting the magnitude of the global aerosol indirect effects arises from those regions with the influence of urban emissions (Sotiropoulou et al., 2007). The study of aerosol-CCN closure and relationships inside and in the outflow of heavily polluted areas is thus important.

East Asia, especially the Jing (Beijing)-Jin (Tianjin)-Ji (Hebei) region, is a fast developing and densely populated region including numerous megacities, where anthropogenic aerosol emissions have increased significantly over recent years (Streets et al., 2008) and where aerosol loading is high and chemical composition is complex (Li et al., 2007a, Xin et al., 2007). The high aerosol loading would have significant influence on radiative properties, cloud microphysics and precipitation (Xu, 2001; Li et al., 2007b; Xia et al., 2007; Rosenfeld et al., 2007; Lau et al., 2008; Li et al., 2011).

Field measurements of CCN have been made in East Asia where megacities are likely to be major sources of pollutants and CCN (Yum et al., 2007; Rose et al., 2008; Gunthe et al., 2009; Yue et al., 2011; Liu et al., 2011; Zhang et al., 2012; Deng et al., 2011; Leng et al., 2013). Despite the significant accomplishments achieved by these

studies, limitations and uncertainties exist. As a recent example for the region of interest, Deng et al. (2011) over predicted the concentration of CCN at a site in the North China Plain by 19% when compared with direct measurements.

The aim of this paper is to study the aerosol hygroscopisity and CCN activity under high aerosol loading in the polluted regions, and get some implications to parameterize CCN number concentrations by using CCN activation ratio (AR) to the proxy of total aerosol particles in the atmosphere. A CDF fit model is applied to both clean and polluted aerosols to probe the influences of size distribution, heterogeneity of chemical composition, and mixing state on CCN activity. The hygroscopicity parameter (κ) is derived using Köhler theory to study aerosols hygroscopicity during clean days and polluted events. In the CCN closure study, besides the parallel observation (PO) closure test, we employ the CCN efficiency spectrum to non-simultaneously CN and CCN observation, namely non-parallel observation (NPO) closure test, to estimate N_{CCN} in order to test the impacts from particle composition. Finally, the relationship between AR and aerosol physical and chemical properties is examined to imply a possibility of CCN parameterization in climate models.

2. Measurement and data

An intensive campaign, named Aerosol-CCN-Cloud Closure Experiment (AC^{3}Exp), was conducted during June and July of 2013 at the Xianghe Atmospheric Observatory (39.798N, 116.958E; 35 m above sea level), located about 60 km southeast of the Beijing metropolitan area. This site is surrounded by agricultural land, densely occupied residences and light industry. Sitting between two megacities (with Beijing to the northwest and Tianjin to the southeast) and less than 5 km west of the local town center (with a population of 50,000), the site experiences frequent pollution plumes. Depending on the wind direction, instruments at the Xianghe site detect

pollutants of urban, rural, or mixed origins, experiencing both fresh biomass burning emissions and advected aged aerosols. More information about the measurement location and meteorological conditions has been described by Li et al. (2007, 2011).

2.1 Instrument and measurement

In the campaign, bulk CCN activation was measured from 1 June to 25 June 2013. Size-resolved CCN was measured from 7 July to 21 July 2013.Aerosl particle size distribution (10-700 nm) was measured from 1 June to 25 June 2013 and 7 July to 21 July 2013. During 1-25 June, a Scanning Mobility Particle Sizer (SMPS) (DMA; TSI 3081, CPC; TSI 3776) was used independently for size distribution measurement; and from 7 to 21 July, it was combined with a Droplet Measurement Technologies - Cloud Condensation Nuclei Counter (DMT-CCNc) (Lance et al., 2006) and used for size-resolved CCN measurement. Aerosol chemical composition was measured from 31 May to 30 June 2013. Therefore, the CCN efficiency spectrum (Fig. 1) is derived from the size-resolved CCN observation from 7 July to 21 July 2013. The aerosol particle size distribution data independently measured by the SMPS from 1 June to 25 June 2013 combing with the derived CCN efficiency spectra (Fig. 1) is used for NPO CCN closure test.

The aerosol inlet for the size distribution measurements was equipped with a TSI Environmental Sampling System (Model 3031200), which consists of a standard PM10 inlet, a sharp-cut PM1 cyclone, and a bundled nafion dryer. After dried through the nafion bundle, the sample flow with relative humidity (RH) of <30% was sent into the SMPS for the aerosol size distribution measurements (10-700 nm). Meanwhile, the CCN number concentrations (N_{CCN}) at different super-saturations were measured, using a continuous-flow CCN counter from the DMT-CCN_C. Each CCN measurement

cycle included three supersaturations: 0.2%, 0.5% and 0.8%. The scanning times for those super-saturations were set as 7, 5, and 5 minutes, respectively.

The size-resolved CCN efficiency spectra were measured by coupling the same DMT-CCN_C used with the SMPS (Rose et al., 2008). In this setup the particles are rapidly dried with RH of <30% upon entering the DMA. Thus, size selection is effectively performed under dry conditions, and the relative deviations in particle diameter should be <1% except for potential kinetic limitations (Mikhailov et al., 2009). The sample flow exiting the DMA was split into two parts, with 0.3 lpm for the CPC and 0.5 lpm for the CCN_C. The DMA, controlled by the TSI-AIM software, scanned one size distribution every five minutes. The CCN_C was operated at a total flow rate of 0.5 lpm with the sheath-to-aerosol flow ratio of 10. The inlet RH for CCN is <30%. During the campaign, the averaging temperature and pressure as measured by the CCN_C sensors were (23.5±1.6) °C and (985.5 ± 3.6) hPa. The deviations were determined by the measurement uncertainties. For each CCN measurement cycle, SS was set to 5 different values: 0.08, 0.11, 0.23, 0.42, and 0.80 %. The completion of a full measurement cycle took 60 min (20 min for the SS= 0.08% and 10 min for each of the rests). The supersaturations of CCN_C were calibrated with ammonium sulfate both before and after the campaign, following Rose's procedures (Rose et al., 2008).

The measurement of non-refractory submicron (NR-PM1) aerosol species including organics, sulfate, nitrate, ammonium, and chloride with an Aerodyne Aerosol Chemical Speciation Monitor (ACSM) (Sun et al., 2012) is also conducted during the campaign. The ACSM uses the same aerosol sampling, vaporization and ionization modules as the Aerosol Mass Spectrometer (AMS) (DeCarlo et al., 2006), but removes the size components, i.e., no size information. During the campaign, ambient aerosol was drawn inside through a ½ inch (outer diameter) stainless steel tube at a

flow rate of ~3 L min^{-1}, of which ~84 cc min^{-1} was sub-sampled into the ACSM. An URG cyclone (Model: URG-2000-30ED) was also supplied in front of the sampling inlet to remove coarse particles with a size cut-off of 2.5 mm. Before sampled into the ACSM, aerosol particles are dried by Silica gel desiccant. The residence time in the sampling tube is ~5 s. The ACSM was operated at a time resolution of ~15 min with a scan rate of mass spectrometer at 500 ms amu^{-1} from m/z 10 to 150. Regarding the calibration of ACSM, the mono-dispersed, size-selected 300 nm ammonium nitrate particles within a range of concentrations were sampled into both the ACSM and a condensation particle counter (CPC). IE was then determined by comparing the response factors of ACSM to the mass calculated with the known particle size and the number concentrations from CPC. Once the IE is determined, the changes of the internal standard naphthalene or air ions, e.g., m/z 28 (N_2^+) or m/z 32 (O_2^+) can be used to account for the degradation of detector. The other details including the instrument, aerosol sampling setup, operations and calibrations were detailed in Sun et al. (2012) and Ng et al. (2011).

In addition to the ACSM, the black carbon (BC) in PM2.5 was simultaneously measured at a time resolution of 5 min by a BC analyzer (Aethalometer, Model AE22, Magee Scientific Corporation). During the experiment period, the campaign area was generally hot and wet, with an average temperature of 23.6°C and an average ambient relative humidity (RH) of 72.3%.

2.2 Data

The raw CCN data for both bulk and size-resolved CCN measurements were firstly filtered according to the instrument recorded parameters (e.g. temperature and flow). A multiple charge correction and transfer function is applied for each CN size

distribution spectrum as well as CCN efficiency spectrum. The CCN activation ratio (AR) is just the ratio of N_{CCN}/N_{CN}. In order to examine the CCN activity under different cases, we classified the size-resolved CCN efficiency data as polluted and background conditions based on the aerosol loading as well as the synchronism surface horizontal winds data. Basically, the polluted conditions are with N_{CN}>15000 cm^{-3} when the airflow came from southeast/east and the background cases are with N_{CN} <15000 cm^{-3} always associated with the winds from west or northwest. N_{CN} is total aerosol number concentrations with particle size range of 10-700 nm. Here, the background refers to a regional background condition which represents a well-mixed atmosphere without influenced by local emissions, e.g biomass burning. Bulk measurement of total CCN number concentrations at SS of 0.2%, 0.5% and 0.8% could lead to considerable underestimation of CCN under polluted conditions (Deng et al.,2011) due to water depletion inside the column (Lathem and Nenes, 2011). Therefore, in this study the data points with N_{CN} >25000 cm^{-3} were excluded. In the closure study, CCN size distributions were calculated by multiplying the fitted CCN efficiency spectra (3-parameter CDF fit) with the aerosol particle number size distribution. Total N_{CCN} was obtained by integrating the CCN over whole size range. The mass concentrations and mass spectra were processed using ACSM standard data analysis software (v 1.5.1.1). The detailed procedures for the data analysis have been described in Ng et al. (2011) and Sun et al. (2012). The campaign averaged mass concentrations of BC are ~4.2 μg m^{-3}, and the averaged mass fraction are about 6%, with maximum of 18% and minimum of 2%.

3. Theory

As proposed by Petters and Kreidenweis (2007), κ can be used to describe the ability to absorb water vapor and act as CCN. Based on Köhler theory (Köhler, 1936), κ

relates the dry diameter of aerosol particles to the critical water vapor SS. According to measurements and thermodynamic models, κ is zero for insoluble materials like soot or mineral dust, however, their hygroscopicity would be changed due to the aging process of the soot and mineral dust and the κ value is thus >0. κ is 0.1 for secondary organic aerosols, 0.6 for ammonium sulfate and nitrate, 0.95-1 for sea salt (Niedermeier et al., 2008), and 1.28 for sodium chloride aerosols. The effective hygroscopicity of mixed aerosols can be approximated by a linear combination of the κ-values of the individual chemical components weighted by the volume or mass fractions, respectively (Kreidenweis et al., 2008; Gunthe et al., 2009). In this study, we calculated κ based on both size-resolved CCN measurements and chemical composition observations during the campaign. The method to derived κ is described below.

3.1 Derivation of κ_a and κ_{cut}

Particle hygroscopicity κ were derived from the measured size resolved CCN activated fraction using κ-Köhler theory (Petters and Kreidenweis, 2007). In κ-Köhler theory, the water vapor saturation ratio over an aqueous solution droplet S is given by:

$$S = \frac{D^3 - D_p^3}{D^3 - D_p^3(1-\kappa)} \exp\left(\frac{4\sigma_w M_w}{RT\rho_w D}\right), \quad (1)$$

where D is the droplet diameter, D_p is the dry diameter of the particle, M_w is the molecular weight of water, σ_w is the surface tension of pure water, ρ_w is the density of water, R *is* the gas constant, and T *is* the absolute temperature. When κ is greater than 0.1, it can be conveniently derived as:

$$\kappa = \frac{4A^3}{27D_p^3 S_c^2} \quad (2)$$

$$A = \frac{4\sigma_w M_w}{RT\rho_w}, \quad (3)$$

where S_c is the particle critical supersaturation and is derived using the approach described by Rose et al., (2008). The characteristic S_c of the size selected CCN is represented by the supersaturation at which AR reaches 50%. For parameters listed above, T =298.15K, R=8.315 J K^{-1} mol^{-1} (gas constant), ρ_w=997.1 kg m^{-3}, M_w=0.018015 kg mol^{-1} and σ_w=0.072 Jm^{-2}. Note that values derived from CCN measurement data through Köhler model calculations assuming the surface tension of pure water have to be regarded as "effective hygroscopicity parameters" that account not only for the reduction of water activity by the solute ("effective Raoult parameters") but also for surface tension effects (Petters and Kreidenweis, 2007).

In this study, a parameter κ_a, which characterizes the average hygroscopicity of CCN-active particles in the size range around activated diameters (D_a), is calculated from the data pairs of SS and D_a based on the κ-Köhler theory. Similarly, a parameter κ_{cut} is also derived from the data pairs of SS and a critical dry particle diameter (D_{cut}) based on the κ-Köhler theory, which characterizes the average hygroscopicity of aerosol particles in the size range around D_{cut}. Note the D_{cut} is the diameter when the AR=50% regardless of maximum activation fraction (MAF) smaller than 1 or equal to 1. Whereas, D_a is the diameter when the AR=MAF/2. The discrepancy of D_{cut} and D_a can reflect the mixing state and chemical heterogeneity of aerosol particles.

3.2 Derivation of κ_{chem}

For a given internal mixture, κ can be predicted by a simple mixing rule on the basis

of chemical volume fractions ε_i (Petters and Kreidenweis, 2007; Gunthe et al., 2009).

$$\kappa_{chem} = \sum_i \varepsilon_i \kappa_i \quad , \qquad (4)$$

where, κ_i and ε_i are the hygroscopicity parameter and volume fraction for the individual (dry) component in the mixture with i the number of components in the mixture. We derive ε_i from the particle chemical composition measured by ACSM. Measurements from ACSM show that the composition of submicron particles was dominated by organics, followed by nitrate, ammonium and sulfate. The contribution of chloride was negligible (with volume fraction of about <2%). The analysis of anion and cation balance suggests that anionic species (NO_3^-, SO_4^{2-}) were essentially neutralized by NH_4^+ over the relevant size range. For refractory species, BC represented a negligible fraction of the total submicron aerosol volume (less than about 3%). The sea salt and dust are usually with coarse mode with particle size of >1 μm (Whitby, 1978), the contribution of such types of aerosols are thus expected to be negligible for the size range of <1000 nm. Therefore, those submicron particles measured by ACSM were mainly consisting of Organics, $(NH_4)_2SO_4$, and NH_4NO_3. The particle hygroscopicity is thus the volume average of the three participating species:

$$\kappa_{chem} = \kappa_{Org} \cdot \varepsilon_{Org} + \kappa_{(NH4)2SO4} \cdot \varepsilon_{(NH4)2SO4} + \kappa_{NH4NO3} \cdot \varepsilon_{NH4NO3}, \quad (5)$$

The values of κ are 0.67 and 0.61 for $(NH_4)_2SO_4$ and NH_4NO_3, respectively derived from previous laboratory experiments (Petters et al., 2007). For Organics, we used a linear function between κ_{Org} and f_{44} derived by Mei et al., (2013) to estimate the κ_{Org} in our study. The formula is written as $\kappa_{Org} = 2.10 \times f_{44} - 0.11$ (Mei et al., 2013). By applying the function, calculated κ_{Org} is 0.115 ± 0.019 during the observed period. Species volume fractions were derived from mass concentrations and densities of

participating species. The densities of $(NH_4)_2SO_4$ and NH_4NO_3 are 1770 kg m^{-3} and 1720 kg m^{-3}, respectively. And the density of organics is 1200 kg m^{-3} (Turpin et al., 2001).

4. Results and discussion

4.1 CDF fit and parameters derived from the CCN efficiency

The spectra of measured CCN efficiency at both polluted and background conditions were fitted with a cumulative Gaussian distribution function (CDF; Rose et al., 2008):

$$f_{N_{CCN}/N_{CN}} = a\left(1 + \mathrm{erf}\left(\frac{D - D_a}{\sigma_a\sqrt{2}}\right)\right), \quad (6)$$

where, the maximum activated fraction MAF=2a, the midpoint activation diameter D_a, and the CDF standard deviation σ_a. The parameters were determined for each spectrum. If MAF=1 by changing parameter "a" to 0.5, the spectrum is characteristic for internally mixed aerosols with homogeneous composition and hygroscopicity of the particles. The 3-parameter fit results represent the average activation properties of the aerosol particle fraction. During the campaign period of AC^{3}Exp 2013, we measured about 1200 size-resolved CCN efficiency spectra for atmospheric aerosols at SS of 0.08% to 0.80%. Fig. 1 shows averaged spectra of measured CCN efficiency at SS of 0.08%, 0.11%, 0.23%, 0.42% and 0.80% for background and polluted conditions. The slope of AR with respect to diameter near D_a in Fig 1 provides information on the heterogeneity of the composition for the size resolved particles. For an ideal case when all CCN-active particles have the same composition and size, a steep change of AR from 0 to MAF would be observed as D reaches D_a. A gradual increase in AR suggests that some of the particles have lower hygroscopicity and/or heterogeneity of the composition and are not able to activate at the given SS than

others. The slope of AR around D_a during polluted events shows gentler increase compared with those under background conditions, especially at low SS. Overall, significant differences of the size-resolved CCN efficiency spectra for polluted and clean conditions at lower SS have been derived. The different shape just suggests aerosols hygroscopisity and CCN activity would be affected by the local sources (e.g. biomass burning).

The three parameters (MAF, D_a, and σ) of CCN efficiency spectra derived from the 3-parameter CDF fits as well as D_{cut}, κ_a and κ_{cut} under polluted and clean conditions were also summarized in Table 1. Da_POL and Da_BG in Table 1 are defined as activation diameter under polluted and clean conditions respectively. Dcut_POL and Dcut_BG are defined as cut-off diameter under polluted and clean conditions respectively.

4.1.1 Activation diameter (D_a)

As expected, D_a decreased with increasing SS under both background and polluted conditions. At a given SS, D_a_POL are larger than D_a_BG. That means the particles at polluted cases would be activated at larger diameter. But, the difference of D_a_POL and D_a_BG reduced and was close to each other with the increasing of SS. Accordingly, D_{cut}_POL and D_{cut}_BG dependence on SS showed similar changes to D_a. But, as stated previously, D_{cut} shows a little bit larger than D_a. Because D_{cut} is defined as the diameter when AR is up to 50%, but based on the CDF fit, the "MAF/2" is smaller than 50% and thus results in a smaller D_a.

4.1.2 Maximum Activated Fraction (MAF)

Generally, aerosols with more uniform and homogenous chemical composition or

with core-shell structure would have a higher MAF. MAF_POL and MAF_BG in Table 1 are defined as maximum activation fraction under polluted and background conditions respectively the MAF_BG and MAF_POL are 0.95-0.98 and 0.94-0.98 respectively at different SS. No significant discrepancies of MAF were observed between polluted and background conditions. It should be noticed that MAF are just closer to 1 but equal to 1. Because MAF for pure ammonium sulphate particles (0.05mol L^{-1}) is equal to 1; Furthermore, the observations have indicated that particles can be able to activate to CCN completely when particle diameter >300 nm even at SS=0.08%. Therefore, a smaller portion (1−MAF, 2-6%) is just caused by the error of CDF fit which will lead to lower MAF than it should be.

4.1.3 CDF standard deviations (σ)

The CDF standard deviations (σ) are general indicators for the extent of external mixing and heterogeneity of particle composition for the investigated aerosol in the size range around D_a. σ_POL and σ_BG in Table 1 are defined as CDF standard deviations under polluted and background conditions respectively. Under ideal conditions, the CDF standard deviations should be zero for an internally mixed, fully mono-disperse aerosol with particles of homogeneous chemical compositions. According to Rose et al.(2008), even after correcting for the DMA transfer function, however, calibration aerosols composed of high-purity ammonium sulfate exhibit small non-zero σ values that correspond to ~3% of D_a. It can be attributed to heterogeneities of the water vapor SS profile in the CCNC or other non-idealities, such as DMA transfer function and particle shape effects. Thus, "heterogeneity parameter" values of σ/D_a=3% indicate internally mixed CCN, whereas higher values indicate external mixtures of particles. σ/Da_POL and σ/Da_BG in Table 1 are

defined as heterogeneity parameter under polluted and background conditions respectively. According to Table 1, σ /D_a_POL and σ /D_a_BG are with values of 17%-30%, which is much higher than 3% observed for pure ammonium sulfate, indicating that the particles were externally mixed with respect to their solute content.

4.2 Derived κ_a dependence on D_a

Fig. 2 shows the dependence of κ_a on D_a under both background and polluted conditions. κ_a_POL and κ_a_BG are defined as average hygroscopicity of CCN-active particles in the size range around D_a under polluted and background conditions. For background days, larger particles were on average more hygroscopic than smaller particles: κ_a_BG increased substantially from about 0.22 at 30-60 nm to about 0.38 at size range of 120-180 nm. Our result is consistent with the field results observed in Guangzhou, South China by Rose et al., (2010). However, compared to κ_a_BG, κ_a_POL exhibited relatively flat trend with the increase of particles size diameter. The κ_a_POL didn't exhibited significant increase but with larger error bars around a given D_p, suggesting the complex and diversities of particle compositions and their mixing state at polluted cases. In this case, larger particles are even less hygroscopic than the smaller particles. One of the possible reason for the changes of κ_a at polluted cases may be due to the high organics freshly emitted from biomass burning (Andreae and Rosenfeld, 2008; Petters et al., 2009; Rose et al., 2010), which would coat on those larger particles and then lead the particles with less hygroscopic. Overall, κ for polluted aerosols are about 20% lower than that of clean aerosols for particles in accumulation size range; for these particles in nucleation or Aitken size range, κ_a for polluted particles is slightly higher than that at background cases. Based on laboratory experiment, Petters et al., (2009) examined the hygroscopic properties of particles

freshly emitted from biomass burning. They found that κ was a function of particle size, with 250 nm particles being generally weakly hygroscopic and sub-100 nm particles being more hygroscopic. During the campaign at Xianghe, the biomass burning aerosols are the lead particles for the selected polluted cases. The laboratory results, to some extent, can thus explain our field measurements. But further investigations including laboratory experiments and field measurements of size-resolved chemical composition are needed to confirm and clarify this. The changes of κ_{cut}_POL and κ_{cut}_BG dependence on D_{cut}, which are not shown here, displayed similar characteristics. But the derived κ_{cut}_POL and κ_{cut}_BG (given in Table 1) are generally slightly smaller than κ_a_POL and κ_a_BG.

4.4 PDF of D_a and κ_a

Fig. 3 exhibits the probability distribution function (PDF) of D_a under background conditions and during polluted events throughout the campaign. D_a_POL are mainly distributed in the ranges of about 185-205, 163-180, 95-120, 65-75 and 45-55 nm at SS of 0.08%, 0.11%, 0.23%, 0.42% and 0.80%, respectively. At each SS, PDF of D_a_POL shows wider distribution than D_a_BG. The PDF for D_a_POL moved several to dozens of nanometer and extended to the side of large particle size at all SS indicating impact by pollutions. In addition, both the D_a_BG and D_a_POL show larger variations at lower SS. This can be explained by two reasons: one is weaken impact (solute effect) of chemical composition on CCN activity at high SS; the other one is probably due to the relatively larger uncertainties for measuring lower SS.

Fig. 4 exhibits the PDF of κ_a under background conditions and during polluted events throughout the campaign. κ_a_POL presents large variations at each size range around D_a. At a given D_p range, they are distributed with two modes. For example, κ_a_POL

for particles around the size diameter of 48 nm is with two hygroscopic peaks of ~0.15 and ~0.23; it is with peak values of ~0.26 and ~0.32 for particles around D_p=198 nm. Because a large amounts of κ_a are <0.3 but a very small portion of particles are with κ_a<0.1 at these cases. Such distribution mode for κ_a at polluted cases thus indicated an externally mixed but with less hygroscopic particles during the polluted cases. Compared to the PDF of κ_a_POL, κ_a_BC displays much less significant variations. It distributed with one mode and with peak values of 0.23, 0.30, 0.35, 0.35 and 0.38 around the size diameter of 46 nm, 64 nm, 92 nm, 152 nm and 179 nm. Few particles are with κ_a<0.3 at D_p>60 nm under background conditions, reflecting that the particles are more hygroscopic with relatively homogeneous composition of the particles under background conditions.

4.5 CCN closure tests

In this section, we compare N_{CCN} observations with corresponding values that were estimated on the basis of aerosol particle number size distributions measured in parallel and non-parallel assuming uniform particles composition. If the estimated and observed N_{CCN} agree quantitatively within the range of their uncertainty, closure is achieved. By using averaged CDF fit curve method with an assumption of uniform chemical composition, CCN size distributions were firstly calculated by multiplying the CCN efficiency spectra with the total aerosol particle (CN) number size distributions measured in parallel and non-parallel. Estimated N_{CCN} were calculated by stepwise integration of the CCN size distributions from 10 to 700 nm.

4.5.1 **Parallel observation (PO) closure tests**

The comparison of estimated and parallel observed N_{CCN} at five SS of 0.08% to 0.80%

is shown in Fig. 5. In this case, a good agreement between estimated and measured N_{CCN} was obtained. The mean slope and correlation coefficient R^2 are 0.99 and 0.97 at the five super saturations. At SS of 0.08% and 0.11%, the results showed a little bit (~3-4%) underestimation of CCN number concentrations. One reason for the slight worse closure between measured and estimated CCN number concentrations at lower SS lies in that size-resolved activation ratios exhibit a larger variability at low SS than that at higher SS. Also, compared to the activated CCN number concentrations at high SS, the N_{CCN} is with a less amounts at low SS, which would lead to larger uncertainties or lower correlation. Overall, the PO closure test indicated that the estimation on a basis of mean CDF fit AR curve methods can estimate the observed N_{CCN} pretty well when SS is high, although uniform and internally mixed chemical composition throughout the size range being assumed.

4.5.2 **Non-parallel observation (NPO) closure tests**

In this study, we also estimate CCN number concentrations based on non-parallel CN size distribution measurements (1-25 June, 2013) by using CDF fit curve derived from the size-resolved CCN measurements (7-21 July, 2013). The comparison of estimated N_{CCN} and the non-parallel measured at SS of 0.2%, 0.5% and 0.8% are shown in Fig. 6. A reasonable agreement between estimated and measured N_{CCN} was obtained by using CDF fit curve method. The lower slope at SS=0.2% indicates that the estimation on a basis of NPO closure underestimates about 7% of the observed N_{CCN}. The closure is considerably improved at higher SS. However, only a reasonable correlation with R^2 of about 0.6-0.8 between estimated and measured N_{CCN} was achieved, which suggests temporal variations both in chemical composition or mixing state of aerosol particles. Overall, the uncertainties in such NPO CCN closure study are about

30%-40%. Thus, it is important to conduct such field experiment to measure CCN under different environmental conditions. Likewise, caution needs to be exercised to use data from any experiment of short periods at a single site to do CCN parameterization for any large-scale applications. It is necessary to conduct long-term CCN measurements at more regional sites, especially those with heavy pollution of high CN.

4.6 Case study: implications of CCN activation combining chemical composition

To understand the behavior of CCN activation under different surrounding circumstance, two cases with total N_{CN}<15000 cm^{-3} and >15000 cm^{-3} during the campaign are selected for investigation, which are defined as background and polluted condition, respectively. Interestingly, bulk CCN activation exhibits completely different changes with N_{CN} from the two cases: the AR at all three SS of 0.2%, 0.5% and 0.8% increase with the increase of N_{CN} at background cases (Fig 7a), whereas they decline with increase of N_{CN} during polluted events (Fig 7b). At background cases, changes of AR are apparently dependence on changes of κ_{chem} (Fig. 7c), showing well correlation between AR_0.2 and κ_{chem} with R^2>0.7 (Fig. 8). Such high correlations between bulk AR and κ_{chem} have been observed when N_{CN} are low during the whole campaign (Fig. 9). In these cases, organics account for relatively low amounts (~30%) of total particle mass concentrations but concentrations of soluble inorganics are high (Fig. 7e). In particular, mass concentration of nitrate is higher than organics accounting for the largest mass fraction of all compositions when κ_{chem} reaches the maximum with a mean value of ~0.45. The *f*44, which is the fraction of total organic mass signal at *m/z* 44, is not correlated with AR (Fig. 7c). The *m/z* 44 signal is due mostly to acids (Takegawa et al., 2007; Duplissy et al., 2011) or

acid-derived species, such as esters, and *f*44 is closely related to the organic oxidation level (i.e., O:C ratio) (Aiken et al.,2008). Usually, the oxidized/aged acids are more hygroscopic and easily activated. Therefore, the deteriorated correlations between *f44* and AR implied that organics at low N_{CN} cases are less hygroscopic. In addition, CN number concentrations at size range of nucleation, Aitken and accumulated mode are also shown in Fig 7g and 7h for background and polluted conditions respectively. In background days, AR at SS=0.2% is more correlated with the changes of N_{CN} at accumulated mode with R^2 of ~0.5 (Fig. 8), suggesting aerosol particles at the size range of >100 nm can be mostly activated. Smaller particles with Aitken diameter of <40 nm at the given SS (0.2%-0.8%) are difficult or cannot be activated, thus there are no correlations indicated in Fig. 7g.

During polluted events, changes of AR didn't displayed apparent dependence on changes of κ_{chem} (Fig. 7d). But AR at SS=0.2% showed moderate correlation with *f*44 with R^2 of ~0.5 (Fig. 8). As stated above, the *f*44 is always related to the organic oxidation level. Usually, the oxidized/aged acids are more hygroscopic and easily activated. The correlation between *f*44 and AR suggested that the significant roles of organics contributions from oxidized or aged aerosols to CCN activity. Because the impact from organics on the particles activation is complicated (Jimenez et al., 2009). In addition, it will introduce definite bias by using a parameterized function derived from observations at other sites with different aerosol types to describe the particle hygroscopicity and activation properties due to the complexity of the organic aerosol fraction and its tendency to evolve with atmospheric oxidative processing and aerosol aging based on previous studies (e.g. Padró et al., 2010; Engelhart et al., 2011, 2012; Asa-Awuku et al., 2011). Similarly, under polluted conditions, AR_0.2 is more correlated with the changes of accumulated mode particles, with R^2 of ~0.3.

Overall, based on the case investigation, one cannot use parameterized formula combining with only N_{CN} to estimate CCN number concentrations. However, if observations such as size-resolve CCN as well as size-resolved chemical compositions are not available, a possibility of using bulk κ_{chem} and $f44$ by combining with bulk $N_{CN>100nm}$ to parameterize CCN number concentrations when with low and high N_{CN} respectively has been implied. But further field investigations or examinations are needed to demonstrate and confirm the relationship between AR and particle size and compositions.

5. Summary and conclusions

Atmospheric aerosol particles acting as CCN are pivotal elements of the hydrological cycle and climate change. In this study, we measured and characterized CCN in relatively clean and polluted air during the AC^{3}Exp campaign conducted at Xianghe, China during summer 2013, with the aim of understanding the CCN activation properties under high aerosol loading in the polluted regions and implying the impacts of particle size and chemical composition on CCN activation ratio to the proxy of total aerosol particles in the atmosphere. Based on the CDF fit method, a gradual increase in AR dependence on D_p suggests that aerosol particles have lower hygroscopicity and heterogeneity of the composition during the campaign. Both D_a and D_{cut} were increased significantly at lower SS (<0.2%) due to pollutions (e.g. biomass burnings); the increase was not observed when SS>0.4%. The value of κ are about 0.31-0.38 for particles in accumulation mode under background conditions and about 20% higher than that derived under polluted conditions; however, κ are about 0.20-0.34 for particles in nucleation or Aitken mode at background cases, showing slightly lower than that during polluted events. Larger particles were on average more hygroscopic than smaller particles. But the case is more complex for particles with

heavy pollutions due to the diversities of particle compositions and mixing state. The low R^2 for the NPO CCN closure test suggests about 30%-40% uncertainties in N_{CCN} prediction that is mainly caused by changes in particle composition. By combining analyses of chemical composition data from ACSM measurement, the relationship between bulk AR and the physical and chemical properties of the atmospheric aerosol is investigated. Based on the case investigation, we conclude that one cannot use parameterized formula combining with only N_{CN} to estimate N_{CCN}. We have implied a possibility of using bulk κ_{chem} and $f44$ by combining with bulk $N_{CN>100nm}$ to parameterize CCN number concentrations when with low and high N_{CN} respectively. Further field investigations or examinations are needed to demonstrate and confirm the relationship between AR and particle size and compositions.

Acknowledgement

We would thank the two reviewers very much for their suggestions and comments which have greatly improved the paper. This work was funded by the National Basic Research Program of China '973' (Grant No. 2013CB955801, 2013CB955804), the National Science Foundation (1118325) and the Fundamental Research Funds for the Central Universities (Grant No. 2013YB35). The support of the entire AC^{3}Exp team has been much appreciated.

References

Aiken, A. C., DeCarlo, P. F., Kroll, J. H., Worsnop, D. R., Huffman, J. A., Docherty, K. S., Ulbrich, I. M., Mohr, C., Kimmel, J. R., Sueper, D., Sun, Y., Zhang, Q., Trimborn, A., Northway, M., Ziemann, P. J., Canagaratna, M. R., Onasch, T. B., Alfarra, M. R., Prevot, A. S. H., Dommen, J., Duplissy, J., Metzger, A., Baltensperger, U., and Jimenez, J. L.: O/C and OM/OC ratios of primary,

secondary, and ambient organic aerosols with high-resolution time-of-flight aerosol mass spectrometry, Environ. Sci. Technol., 42, 4478–4485, 2008.

Albrecht, B. A.: Aerosols, clouds and microphysics, Science, 245, 1227–1230, 1989.

Alfarra, M. R., Coe, H., Allan, J. D., Bower, K. N., Boudries, H., Canagaratna, M. R., Jimenez, J. L., Jayne, J. T., Garforth, A. A., Li, S.-M., and Worsnop, D. R.: Characterization of urban and rural organic particulate in the Lower Fraser Valley using two Aerodyne Aerosol Mass Spectrometers., Atmos. Environ., 38, 5745–5758, 2004.

Andreae, M. O. and Rosenfeld, D.: Aerosol-cloud precipitation interactions. Part 1. The nature and sources of cloud-active aerosols, Earth. Sci. Rev., 89, 13-41, doi:10.1016/j.earscirev.2008.03.001, 2008.

Anttila, T. and Kerminen, V. M.: On the contribution of Aitken mode particles to cloud droplet populations at continental background areas – a parametric sensitivity study, Atmos. Chem. Phys., 7, 4625–4637, 2007.

Asa-Awuku, A., Moore, R. H., Nenes, A., Bahreini, R., Holloway, J. S., Brock, C. A., Middlebrook, A. M., Ryerson, T., Jimenez, J., DeCarlo, P., Hecobian, A., Weber, R., Stickel, R., Tanner, D. J., and Huey, L. G.: Airborne cloud condensation nuclei measurements during the 2006 Texas Air Quality Study, J. Geophys. Res., 116, D11201, doi:10.1029/2010JD014874, 2011.

Bougiatioti, A., Fountoukis, C., Kalivitis, N., Pandis, S. N., Nenes, A., and Mihalopoulos, N.: Cloud condensation nuclei measurements in the marine boundary layer of the eastern Mediterranean: CCN closure and droplet growth kinetics. Atmos. Chem. Phys., 9, 7053–7066, 2009.

Bougiatioti, A., Nenes, A., Fountoukis, C., Kalivitis, N., Pandis, S. N., and Mihalopoulos, N.: Size-resolved CCN distributions and activation kinetics of aged

continental and marine aerosol, Atmos. Chem. Phys., 11, 8791-8808, doi:10.5194/acp-11-8791-2011, 2011.

Chuang, P. Y., Collins, D. R., Pawlowska, H., Snider, J. R., Jonsson, H. H., Brenguier, J. L., Flagan, R. C., and Seinfeld, J. H.: CCN measurements during ACE-2 and their relationship to cloud microphysical properties, Tellus B, 52, 843–867, 2000.

Clarke, A., McNaughton, C., Kasputin, V. N., Shinozuka, Y., Howell, S., Dibb, J., Zhou, J., Anderson, B., Brekhovskikh, V., Turner, H., and Pinkerton, M.: Biomass burning and pollution aerosol over North America: Organic components and their influence on spectral optical properties and humidification response, J. Geophys. Res., 112, D12S18, doi:10.1029/2006JD007777, 2007.

DeCarlo, P.F., Kimmel, J.R., Trimborn, A., Northway, M.J., Jayne, J.T., Aiken, A.C.,Gonin, M., Fuhrer, K., Horvath, T., Docherty, K.S., Worsnop, D.R., Jimenez, J.L.: Field-deployable, high-resolution, time-of-flight aerosol mass spectrometer. Anal. Chem., 78, 8281-8289, 2006.

Deng, Z., Zhao, C., Ma, N., Liu, F., Ran, L., Xu, W., Liang, Z., Liang, S., Huang, M., Ma, X., Zhang, Q., Quan, J., and Yan, P.: Size- resolved and bulk activation properties of aerosols in the North China Plain. Atmos. Chem. Phys., 11, 3835-3846, 2011.

Deng, Z., Zhao, C., Ma, N., Ran, L., Zhou, G., Lu, D., and Zhou, X.: An examination of parameterizations for the CCN number concentration based on in situ measurements of aerosol activation properties in the North China Plain, Atmos. Chem. Phys., 13, 6227–6237, doi:10.5194/acp-13-6227-2013, 2013.

Dusek, U., Covert, D. S., Wiedensohler, A., Neususs, C., Weise, D., and Cantrell, W.: Cloud condensation nuclei spectra derived from size distributions and hygroscopic properties of the aerosol in coastal south-west Portugal during ACE-2, Tellus B, 55,

35–53, 2003.

Dusek, U., Frank, G. P., Hildebrandt, L., Curtius, J., Schneider, J., Walter, S., Chand, D., Drewnick, F., Hings, S., Jung, D., Borrmann, S., and Andreae, M. O.: Size matters more than chemistry for cloud-nucleating ability of aerosol particles, Science, 312, 1375–1378, 2006a.

Dusek, U., Reischl, G. P., and Hitzenberger, R.: CCN activation of pure and coated carbon black particles, Environ. Sci. Technol., 40, 1223–1230, 2006b.

Duplissy, J., DeCarlo, P. F., Dommen, J., Alfarra, M. R., Metzger, A., Barmpadimos, I., Prevot, A. S. H.,Weingartner, E., Tritscher, T., Gysel, M., Aiken, A. C., Jimenez, J. L., Canagaratna, M. R., Worsnop, D. R., Collins, D. R., Tomlinson, J., and Baltensperger, U.: Relating hygroscopicity and composition of organic aerosol particulate matter, Atmos. Chem. Phys., 11, 1155–1165, doi:10.5194/acp-11-1155-2011, 2011.

Engelhart, G. J., Moore, R. H., Nenes, A., and Pandis, S. N.: Cloud condensation nuclei activity of isoprene secondary organic aerosol, J. Geophys. Res., 116, D02207, doi:10.1029/2010JD014706, 2011.

Engelhart, G. J., Hennigan, C. J., Miracolo, M. A., Robinson, A. L., and Pandis, S. N.: Cloud condensation nuclei activity of fresh primary and aged biomass burning aerosol, Atmos. Chem. Phys., 12, 7285–7293, doi:10.5194/acp-12-7285-2012, 2012.

Ervens, B., Feingold, G., and Kreidenweis, S.: Influence of watersoluble organic carbon on cloud drop number concentration., J. Geophys. Res., 110, D18211, doi:10.1029/2004JD005634, 2005.

Feingold, G.: Modeling of the first indirect effect: Analysis of measurement requirements, Geophys. Res. Lett., 30(19), doi:10.1029/2003GL017967, 2003.

Gasparini, R., Collins, D. R., Andrews, E., Sheridan, P. J., Ogren, J. A., and Hudson, J. G.: Coupling aerosol size distributions and size-resolved hygroscopicity to predict humidity-dependent optical properties and cloud condensation nuclei spectra., J. Geophys. Res., 111, D05S13, doi:10.1029/2005JD006092, 2006.

Gunthe, S. S., King, S. M., Rose, D., Chen, Q., Roldin, P., Farmer, D. K., Jimenez, J. L., Artaxo, P., Andreae, M. O., Martin, S. T., and Pöschl, U.: Cloud condensation nuclei in pristine tropical rainforest air of Amazonia: size-resolved measurements and modeling of atmospheric aerosol composition and CCN activity, Atmos. Chem. Phys., 9, 7551-7575, doi:10.5194/acp-9-7551-2009, 2009.

Hartz, K. E. H., Tischuk, J. E., Chan, M. N., Chan, C. K., Donahue, N. M., and Pandis, S. N.: Cloud condensation nuclei activation of limited solubility organic aerosol, Atmos. Environ., 40, 605–617, 2006.

Hudson, J.: Variability of the relationship between particle size and cloud-nucleating ability, Geophys. Res. Lett., 34, L08801, doi:10.1029/2006GL028850, 2007.

IPCC: Climate change 2007: Scientific basis, Fourth assessment of the Inter-governmental Panel on Climate Change, Cambridge Univ. Press, New York, 2007.

IPCC: Climate change 2013: Scientific basis, Fifth assessment of the Inter-governmental Panel on Climate Change, Cambridge Univ. Press, New York, 2013.

Jimenez, J. L., Canagaratna, M. R., Donahue, N. M., Prevot, A. S. H., Zhang, Q., Kroll, J. H., DeCarlo, P. F., Allan, J. D., Coe, H., Ng, N. L., Aiken, A. C., Docherty, K. S., Ulbrich, I. M., Grieshop, A. P., Robinson, A. L., Duplissy, J., Smith, J. D., Wilson, K. R., Lanz, V. A., Hueglin, C., Sun, Y. L., Tian, J., Laaksonen, A., Raatikainen, T., Rautiainen, J., Vaattovaara, P., Ehn, M., Kulmala, M., Tomlinson,

J. M., Collins, D. R., Cubison, M. J., Dunlea, E. J., Huffman, J. A., Onasch, T. B., Alfarra, M. R., Williams, P. I., Bower, K., Kondo, Y., Schneider, J., Drewnick, F., Borrmann, S., Weimer, S., Demerjian, K., Salcedo, D., Cottrell, L., Griffin, R., Takami, A., Miyoshi, T., Hatakeyama, S., Shimono, A., Sun, J. Y., Zhang, Y. M., Dzepina, K., Kimmel, J. R., Sueper, D., Jayne, J. T., Herndon, S. C., Trimborn, A. M., Williams, L. R., Wood, E. C., Middlebrook, A. M., Kolb, C. E., Baltensperger, U., and Worsnop, D. R.: Evolution of Organic Aerosols in the Atmosphere, Science, 326, 1525–1529, 2009.

Köhler, H.: The nucleus in and growth of hygroscopic droplets, Trans. Faraday Soc., 32, 1152–1161, doi:10.1039/TF9363201152, 1936.

Kreidenweis, S. M., Petters, M. D., and DeMott, P. J.: Single-parameter estimates of aerosol water content, Environ. Res. Lett., 3, 035002 doi:10.1088/1748-9326/3/3/035002, 2008.

Kuwata, M., Kondo, Y., Mochida, M., Takegawa, N., and Kawamura, K.: Dependence of CCN activity of less volatile particles on the amount of coating observed in Tokyo, J. Geophys. Res., 112, D11207, doi:10.1029/2006JD007758, 2007.

Kuwata, M., Kondo, Y., Miyazaki, Y., Komazaki, Y., Kim, J. H., Yum, S. S., Tanimoto, H., and Matsueda, H.: Cloud condensation nuclei activity at Jeju Island, Korea in spring 2005, Atmos. Chem. Phys., 8, 2933–2948, doi:10.5194/acp-8-2933-2008, 2008.

Lance, S., Medina, J., Smith, J., and Nenes, A.: Mapping the operation of the DMT continuous flow CCN counter, Aerosol Sci. Technol., 40 , 242–254, 2006.

Lathem, T. L., Beyersdorf, A. J., Thornhill, K. L., Winstead, E. L., Cubison, M. J., Hecobian, A., Jimenez, J. L., Weber, R. J., Anderson, B. E., and Nenes, A.:

Analysis of CCN activity of Arctic aerosol and Canadian biomass burning during summer 2008, Atmos. Chem. Phys., 13, 2735-2756, doi:10.5194/acp-13-2735-2013, 2013.

Lau, K. M., Ramahathan, V., Wu, G., Li, Z., Tsay, S. C., Hsu, C., Sikka, R., Holben, B., Lu,D., Tartari, G., Chin, M., Koudelova, P., Chen, H., Ma, Y., Huang, J., Taniguchi, K., and Zhang, R.: The joint aerosol monsoon experiment: A new challenge for monsoon climate research, Bull. Am. Meteorol. Soc., 89, 369–383, doi:10.1175/BAMS-89-3-369, 2008.

Lee, S. H., Murphy, D. M., Thomson, D. S., and Middlebrook, A. M.: Nitrate and oxidized organic ions in single particle mass spectra during the 1999 Atlanta Supersite Project, J. Geophys. Res., 108, 8417, doi:10.1029/2001JD001455, 2003.

Lee, Y. S., Collins, D. R., Li, R. J., Bowman, K. P., and Feingold, G.: Expected impact of an aged biomass burning aerosol on cloud condensation nuclei and cloud droplet concentrations, J. Geophys. Res., 111, D22204, doi:10.1029/2005JD006464, 2006.

Leng, C., Cheng, T., Chen, J., Zhang, R., Tao, J., Huang, G., Zha, S., Zhang, M., Fang, W., Li, X., Li, L.: Measurements of surface cloud condensation nuclei and aerosol activity in downtown Shanghai. Atmos. Environ., 69, 354-361, 2013.

Liu, J., Zheng, Y., Li, Z., and Cribb, M.: Analysis of cloud condensation nuclei properties at a polluted site in southeastern China during the AMF‐China Campaign, J. Geophys. Res., 116, D00K35, doi:10.1029/2011JD016395, 2011.

Li, Z., Xia, X., Cribb, M., Mi, W., Holben, B., Wang, P., Chen, H., Tsay, S-C., Eck, T. F., Zhao, F., Dutton, E. G., and Dickerson, R. E.: Aerosol optical properties and their radiative effects in northern China, J. Geophys. Res., 112, D22S01, doi:10.1029/ 2006JD007382, 2007b.

Li, Z., Li, C., Chen, H., Tsay, S.-C., Holben, B., Huang, J., Li, B., Maring, H., Qian, Y., Shi, G., Xia, X., Yin, Y., Zheng, Y., and Zhuang, G.: East Asian Studies of Tropospheric Aerosols and Impact on Regional Climate (EAST‐AIRC): An overview, J. Geophys. Res., 116, D00K34, doi:10.1029/2010JD015257, 2011.

Li, Z., Chen, H., Cribb, M., Dickerson, R. E., Holben, B., Li, C., Lu, D., Luo, Y., Maring, H., Shi, G., Tsay, S.-C., Wang, P., Wang, Y., Xia, X., Zheng, Y., Yuan, T., and Zhao, F.: Preface to special section on East Asian Studies of Tropospheric Aerosols: An International Regional Experiment (EASTAIRE), J. Geophys. Res., 112, D22S00, doi:10.1029/2007JD008853, 2007a.

Ma, Y., Brooks, S. D., Vidaurre, G., Khalizov, A. F., Wang, L.: Rapid modification of cloud-nucleating ability of aerosols by biogenic emissions, Geophys. Res. Lett. 40, 6293-6297, doi: 10.1002/2013GL057895, 2013.

Mircea, M., Facchini, M. C., Decesari, S., Cavalli, F., Emblico, L., Fuzzi, S., Vestin, A., Rissler, J., Swietlicki, E., Frank, G., Andreae, M. O., Maenhaut, W., Rudich, Y., and Artaxo, P.: Importance of the organic aerosol fraction for modeling aerosol hygroscopic growth and activation: a case study in the Amazon Basin, Atmos. Chem. Phys., 5, 3111–3126, 2005, http://www.atmos-chem-phys.net/5/3111/2005/.

Mei, F., Setyan, A., Zhang, Q., and Wang, J.: CCN activity of organic aerosols observed downwind of urban emissions during CARES, Atmos. Chem. Phys., 13, 12155–12169,doi:10.5194/acp-13-12155-2013, 2013.

Mikhailov, E., Vlasenko, S., Martin, S. T., Koop, T., and P¨ oschl, U.: Amorphous and crystalline aerosol particles interacting with water vapor: conceptual framework and experimental evidence for restructuring, phase transitions and kinetic limitations, Atmos. Chem. Phys., 9, 9491–9522, doi:10.5194/acp-9-9491-2009, 2009.

Niedermeier, D., Wex, H., Voigtländer, J., Stratmann, F., Brüggemann, E., Kiselev, A., Henk, H., and Heintzenberg, J.: LACIS-measurements and parameterization of sea-salt particle hygroscopic growth and activation, Atmos. Chem. Phys., 8, 579-590, doi:10.5194/acp-8-579-2008, 2008.

Ng, N. L., Herndon, S. C., Trimborn, A., Canagaratna, M. R., Croteau, P. L., Onasch, T. B., Sueper, D.,Worsnop, D. R., Zhang, Q., Sun, Y. L., and Jayne, J. T.: An Aerosol Chemical Speciation Monitor (ACSM) for Routine Monitoring of the Composition and Mass Concentrations of Ambient Aerosol, Aerosol Sci. Tech., 45, 770–784, 2011.

Paramonov, M., Aalto, P. P., Asmi, A., Prisle, N., Kerminen, V.-M., Kulmala, M., and Petäjä, T.: The analysis of size-segregated cloud condensation nuclei counter (CCNC) data and its implications for aerosol-cloud interactions, Atmos. Chem. Phys. Discuss., 13, 9681-9731, doi:10.5194/acpd-13-9681-2013, 2013.

Padró, L. T., Tkacik, D., Lathem, T. L., Hennigan, C. J., Sullivan, A. P., Weber, R. J., Huey, L. G., and Nenes, A.: Investigation of cloud condensation nuclei properties and droplet growth kinetics of the water-soluble aerosol fraction in Mexico City, J. Geophys. Res., 115, D09204, doi:10.1029/2009JD013195, 2010.

Petters, M. D., and Kreidenweis, S. M.: A single parameter representation of hygroscopic growth and cloud condensation nucleus activity, Atmos. Chem. Phys., 7, 1961–1971, doi:10.5194/acp-7-1961-2007, 2007.

Petters, M. D., Carrico, C. M., Kreidenweis, S. M., Prenni, A. J., DeMott, P. J., Collett, J. L., and Moosmu¨ller, H.: Cloud condensation nucleation activity of biomass burning aerosol, J. Geophys. Res., 114, D22205, doi:10.1029/2009JD012353, 2009.

Pringle, K. J., Tost, H., Pozzer, A., Pöschl, U., and Lelieveld, J.: Global distribution of the effective aerosol hygroscopicity parameter for CCN activation, Atmos. Chem. Phys., 10, 5241-5255, doi:10.5194/acp-10-5241-2010, 2010.

Quinn, P. K., Bates, T. S., Coffman, D. J., and Covert, D. S.: Influence of particle size and chemistry on the cloud nucleating properties of aerosols, Atmos. Chem. Phys., 8, 1029–1042, 2008, http://www.atmos-chem-phys.net/8/1029/2008/.

Raymond, T. M., and Pandis, S. N.: Cloud activation of single component organic aerosol particles, J. Geophys. Res., 107, 4787, doi:10.1029/2002JD002159, 2002.

Rissler, J., Swietlicki, E., Zhou, J., Roberts, G., Andreae, M. O., Gatti, L. V., and Artaxo, P.: Physical properties of the submicrometer aerosol over the Amazon rain forest during the wet to dry season transition – comparison of modeled and measured CCN concentrations, Atmos. Chem. Phys., 4, 2119–2143, http://www.atmos-chem-phys.net/4/2119/2004/, 2004.

Roberts, G. C., Artaxo, P., Zhou, J. C., Swietlicki, E., and Andreae, M. O.: Sensitivity of CCN spectra on chemical and physical properties of aerosol: A case study from the Amazon Basin, J. Geophys. Res., 107, 8070, doi:10.1029/2001JD000583, 2002.

Rose, D., Nowak, A., Achtert, P.,Wiedensohler, A., Hu, M., Shao, M., Zhang, Y., Andreae, M. O., and P¨ oschl, U.: Cloud condensation nuclei in polluted air and biomass burning smoke near the mega-city Guangzhou, China – Part 1: Size-resolved measurements and implications for the modeling of aerosol particle hygroscopicity and CCN activity, Atmos. Chem. Phys., 10, 3365–3383, doi:10.5194/acp-10-3365-2010, 2010.

Rose, D., Gunthe, S. S., Su, H., Garland, R. M., Yang, H., Berghof, M., Cheng, Y. F., Wehner, B., Achtert, P., Nowak, A., Wiedensohler, A., Takegawa, N., Kondo, Y., Hu, M., Zhang, Y., Andreae, M. O., and Pöschl, U.: Cloud condensation nuclei in

polluted air and biomass burning smoke near the mega-city Guangzhou, China – Part 2: Size-resolved aerosol chemical composition, diurnal cycles, and externally mixed weakly CCN-active soot particles, Atmos. Chem. Phys., 11, 2817-2836, doi:10.5194/acp-11-2817-2011, 2011.

Rose, D., Gunthe, S. S., Mikhailov, E., Frank, G. P., Dusek, U., Andreae, M. O., and Poschl, U.: Calibration and measurement uncertainties of a continuous-flow cloud condensation nuclei counter (DMT-CCNC): CCN activation of ammonium sulfate and sodium chloride aerosol particles in theory and experiment, Atmos. Chem. Phys., 8, 1153–1179, 2008, http://www.atmos-chem-phys.net/8/1153/2008/.

Rosenfeld, D., Dai, J., Yu, X., Yao, Z., Xu, X., Yang, X., and Du, C.: Inverse relations between amounts of air pollution and orographic precipitation, Science, 315(5817), 1396–1398, doi:10.1126/science.1137949, 2007.

Salcedo, D., Onasch, T. B., Dzepina, K., Canagaratna, M. R., Zhang, Q., Huffman, J. A., DeCarlo, P. F., Jayne, J. T., Mortimer, P., Worsnop, D. R., Kolb, C. E., Johnson, K. S., Zuberi, B., Marr, L. C., Volkamer, R., Molina, L. T., Molina, M. J., Cardenas, B., Bernabe, R. M., Marquez, C., Gaffney, J. S., Marley, N. A., Laskin, A., Shutthanandan, V., Xie, Y., Brune,W., Lesher, R., Shirley, T., and Jimenez, J. L.: Characterization of ambient aerosols in Mexico City during the MCMA-2003 campaign with Aerosol Mass Spectrometry: results from the CENICA Supersite, Atmos. Chem. Phys., 6, 925–946, 2006.

Sotiropoulou, R. E. P., Nenes, A., Adams, P. J., and Seinfeld, J. H.: Cloud condensation nuclei prediction error from application of K¨ohler theory: Importance for the aerosol indirect effect, J. Geophys. Res., 112, D12202, doi:10.1029/2006JD007834, 2007.

Streets, D. G., Yu, C., Wu, Y., Chin, M., Zhao, Z., Hayasaka, T., and Shi, G.: Aerosol

trends over China, 1980–2000, Atmos. Res., 88, 174–182, doi:10.1016/j.atmosres.2007.10.016, 2008.

Stroud, C. A., Nenes, A., Jimenez, J. L., DeCarlo, P., Huffman, J. A., Bruintjes, R., Nemitz, E., Delia, A. E., Toohey, D. W., Guenther, A. B., and Nandi, S.: Cloud Activating Properties of Aerosol Observed during CELTIC, J. Atmos. Sci., 64, 441–459, 2007.

Sun, Y., Wang, Z., Dong, H., Yang, T., Li, J., Pan, X., Chen, P., and Jayne, J. T.: Characterization of summer organic and inorganic aerosols in Beijing, China with an Aerosol Chemical Speciation Monitor, Atmos. Environ., 51, 250–259, doi:10.1016/j.atmosenv.2012.01.013, 2012.

Takegawa, N., Miyakawa, T., Kawamura, K., and Kondo, Y.: Contribution of selected di-carboxylic and omega-oxocarboxylic acids in ambient aerosol to the m/z 44 signal of an aerodyne aerosol mass spectrometer, Aerosol Sci. Technol., 41, 418–437, doi:10.1080/02786820701203215, 2007.

Turpin, B. J., and Lim, H. J.: Species contributions to PM2.5 mass concentrations: Revisiting common assumptions for estimating organic mass, Aerosol Sci. Tech., 35, 602-610, 2001.

Twomey, S.: Pollution and planetary albedo, Atmos. Environ., 8, 1251–1256, 1974.

Twomey, S.: The influence of pollution on the shortwave albedo of clouds, J. Atmos. Sci., 34, 1149–1152, doi:10.1175/1520-0469(1977)034<1149:TIOPOT>2.0.CO;2, 1977.

VanReken, T. M., Ng, N. L., Flagan, R. C., and Seinfeld, J. H.: Cloud condensation nucleus activation properties of biogenic secondary organic aerosol, J. Geophys. Res., 110, D07206, doi:10.1029/2004JD005465, 2005.

VanReken, T. M., Rissman, T. A., Roberts, G. C., Varutbangkul, V., Jonsson, H. H.,

Flagan, R. C., and Seinfeld, J. H.: Toward aerosol/cloud condensation nuclei (CCN) closure during CRYSTAL-FACE, J. Geophys. Res., 108, 4633, doi:10.1029/2003JD003582, 2003.

Varutbangkul, V., Brechtel, F. J., Bahreini, R., Ng, N. L., Keywood, M. D., Kroll, J. H., Flagan, R. C., Seinfeld, J. H., Lee, A., and Goldstein, A. H.: Hygroscopicity of secondary organic aerosols formed by oxidation of cycloalkenes, monoterpenes, sesquiterpenes, and related compounds, Atmos. Chem. Phys., 6, 2367–2388, 2006.

Whitby, K., T.: The physical characteristics of sulfur aerosols. Atmos. Environ., 12, 135-159, 1967, Online publication date: 1-Jan-1978, 1978.

Xia, X., Li, Z., Holben, B., Wang, P., Eck, T., Chen, H., Cribb, M., and Zhao, Y.: Aerosol optical properties and radiative effects in the Yangtze Delta region of China, J. Geophys. Res., 112, D22S12, doi:10.1029/2007JD008859, 2007.

Xin, J., Wang, Y., Li, Z., Wang, P., Hao, W., Nordgren, B. L., Wang, S., Liu, G., Wang, L., Wen, T., Sun, Y., Hu, B.: AOD and Angstrom exponent of aerosols observed by the Chinese Sun Hazemeter Network from August 2004 to September 2005, J. Geophys. Res., 112, D05203, doi:10.1029/2006JD007075, 2007.

Xu, Q.: Abrupt change of the mid‐summer climate in central east China by the influence of atmospheric pollution, Atmos. Environ., 35, 5029–5040, doi:10.1016/S1352-2310(01)00315-6, 2001.

Yue, D. L., Hu, M., Zhang, R. J., Wu, Z. J., Su, H., Wang, Z. B., Peng, J. F., He, L.Y., Huang, X. F., Gong, Y. G., and Wiedensohler, A.: Potential contribution of new particle formation to cloud condensation nuclei in Beijing, Atmos. Environ., 45, 6070-6077, 2011.

Yum, S. S., Roberts, G., Kim, J. H., Song, K., and Kim, D.: Submicron aerosol size distributions and cloud condensation nuclei concentrations measured at Gosan,

Korea, during the Atmospheric Brown Clouds–East Asian Regional Experiment 2005, J. Geophys. Res., 112, D22S32, doi:10.1029/2006JD008212, 2007.

Zhang, Q., Meng, J., Quan, J., Gao, Y., Zhao, D., Chen, P., and He, H.: Impact of aerosol composition on cloud condensation nuclei activity, Atmos. Chem. Phys., 12, 3783-3790, doi:10.5194/acp-12-3783-2012, 2012.

Zhang, Q., Stanier, C. O., Canagaratna, M. C., Jayne, J. T., Worsnop, D. R., Pandis, S. N., and Jimenez, J. L.: Insights into the Chemistry of New Particle Formation and Growth Events in Pittsburgh Based on Aerosol Mass Spectrometry, Environ. Sci. Technol., 38, 4797–4809, 2004.

Zhang, R., Khalizov, A. F., Pagels, J., Zhang, D., Xue, H., and McMurry, P. H.: Variability in morphology, hygroscopic and optical properties of soot aerosols during internal mixing in the atmosphere, Proc. Natl. Acad. Sci. USA 105, 10291–10296, 2008.

Table captions:

Table 1. Characteristic of spectra basic spectral parameters for polluted and background aerosols during the campaign for different super saturation. Quantities are midpoint activation diameters (D_a, D_{cut}), maximum activated fractions (MAF), CDF standard deviations (σ), heterogeneity parameters (σ/D_a), hygroscopicity parameters (κ_a, κ_{cut}).

Figure captions:

Fig. 1. Averaged measured CCN efficiency spectra by the 3-parameter CDF fit at SS of 0.08%, 0.11%, 0.23%, 0.42% and 0.80% for polluted and background conditions during the size-resolved CCN measurements period.

Fig. 2. Derived hygroscopicity parameters, κ_a against the particle diameters for polluted and background conditions. Percent changes of κ_a due to the pollutions are plotted here.

Fig. 3 Probability distribution (PDF) of D_a under background and polluted conditions at five SS of 0.08-0.80% during the size-resolved CCN measurements period.

Fig. 4 PDF of κ_{cut} under background and polluted conditions at different particle size ranges during the size-resolved CCN measurements period.

Fig. 5 Estimated N_{CCN} plotted against the observed N_{CCN} in parallel observation (PO) closure test. The green solid line is the 1:1 line.

Fig. 6 Estimated N_{CCN} plotted against the observed N_{CCN} in Non-parallel observation (NPO) closure test. The green solid line is the 1:1 line, and the dashed green lines indicate the band of about ±30% deviation of N_{CCN}-estimated from N_{CCN}-observed.

Fig. 7 Two selected cases of background conditions (22-23 June, 2013) with N_{CN} of <15000 cm^{-3} (left) and polluted events (14-15 June, 2013) with N_{CN} > 15000 cm^{-3} (right) during the campaign. Bulk CCN activation ratios (AR) at all three supersaturations of 0.2%, 0.5% and 0.8% against N_{CN} in clear days and polluted days are shown in Fig 7a and Fig. 7b respectively. Diurnal variations of AR, derived κ_{chem} and fraction of total organic mass signal at *m/z* 44 (f44) are shown in Fig. 7c (background conditions) and Fig. 7d (polluted events). Mass concentrations of black carbon (BC), organics, nitrate (NO_3^-), ammonium (NH_4^+), sulfate (SO_4^{2-}), chloride (Cl^-) irons etc. are shown in Fig. 7e (background conditions) and Fig.7f (polluted events). N_{CN} at size range of nucleation, Aitken and accumulated mode are shown in Fig 7g and Fig. 7h for background conditions and polluted events respectively.

Fig. 8 Correlations of AR with κ_{chem}, *f*44 and N_{CN}_Acc. at background (with low N_{CN}) and polluted (with high N_{CN}) cases. The AR is measured at SS=0.2%, the N_{CN}_Acc. is CN number concentrations at accumulated modes.

Fig. 9. An example for temporal variations of bulk AR at spersaturation of 0.5%, derived κ_{chem} and N_{CN} during the campaign (19-24 June, 2013). The periods (with low N_{CN}) when high correlations between bulk AR and κ_{chem} were observed were marked by rectangles in light green color.

Table 1. Characteristic of spectra basic spectral parameters for polluted and background aerosols during the campaign for different super saturation. Quantities are midpoint activation diameters (D_a, D_{cut}), maximum activated fractions (MAF), CDF standard deviations (σ), heterogeneity parameters (σ/D_a), hygroscopicity parameters (κ_a, κ_{cut}).

SS	D_a_POL	D_{cut}_POL	MAF_POL	σ_POL	σ/D_a_POL	κ_a_POL	κ_{cut}_POL	D_a_BG	D_{cut}_BG	MAF_BG	σ_BG	σ/D_a_BG	κ_a_BG	κ_{cut}_BG
0.079%	190.43±6.11	191.27±5.23	0.98±0.01	33.34±4.49	0.17±0.02	0.32±0.03	0.31±0.02	178.68±4.22	180.22±3.97	0.98±0.01	32.73±2.07	0.18±0.01	0.38±0.02	0.37±0.03
0.109%	161.80±15.10	162.93±15.14	0.98±0.01	38.61±7.62	0.22±0.03	0.26±0.05	0.26±0.05	151.03±2.90	153.62±2.69	0.97±0.01	28.56±1.97	0.19±0.01	0.33±0.02	0.31±0.02
0.228%	94.05±8.47	95.31±7.01	0.96±0.01	27.87±6.30	0.26±0.04	0.31±0.05	0.30±0.05	91.75±2.48	93.40±2.27	0.96±0.00	18.81±1.53	0.20±0.01	0.34±0.02	0.32±0.02
0.423%	63.33±3.65	64.76±3.14	0.94±0.01	18.02±2.84	0.26±0.03	0.30±0.04	0.28±0.04	64.06±1.24	65.86±1.13	0.95±0.00	16.21±0.81	0.25±0.01	0.29±0.01	0.27±0.02
0.797%	44.78±2.51	47.55±2.65	0.94±0.01	14.08±0.98	0.29±0.01	0.24±0.03	0.20±0.04	45.67±1.29	47.25±1.16	0.95±0.01	13.82±1.17	0.30±0.02	0.22±0.02	0.20±0.02

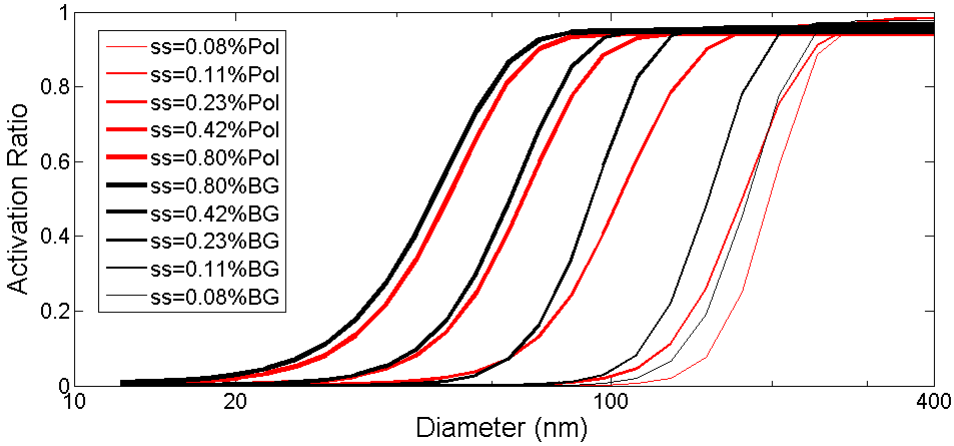

Fig. 1. Averaged measured CCN efficiency spectra by the 3-parameter CDF fit at SS of 0.08%, 0.11%, 0.23%, 0.42% and 0.80% for polluted and background conditions during the size-resolved CCN measurements period.

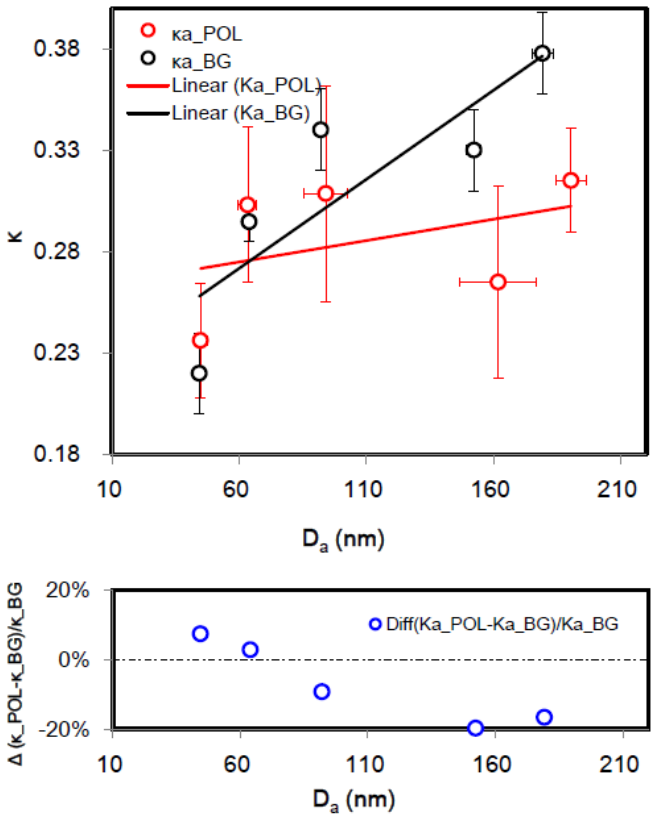

Fig. 2. Derived hygroscopicity parameters, κ_a against the particle diameters for polluted and background conditions. Percent changes of κ_a due to the pollutions are plotted here.

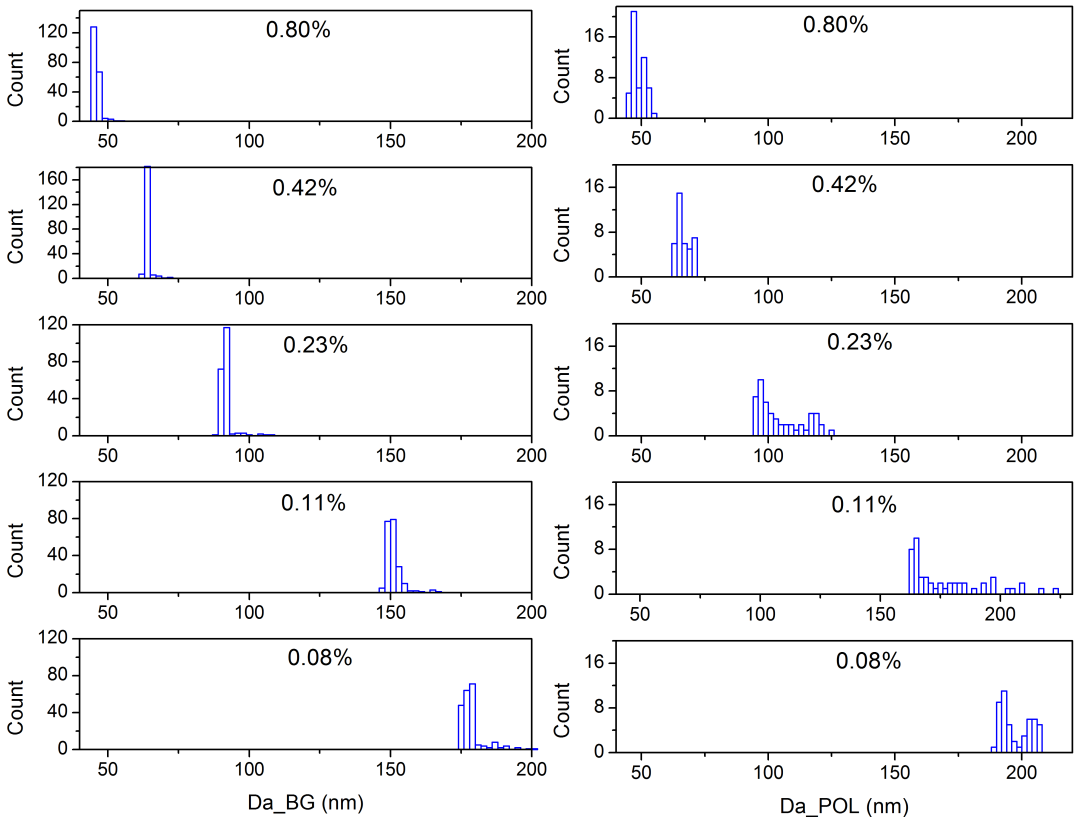

Fig. 3 Probability distribution (PDF) of D_a under background and polluted conditions at five SS of 0.08-0.80% during the size-resolved CCN measurements period.

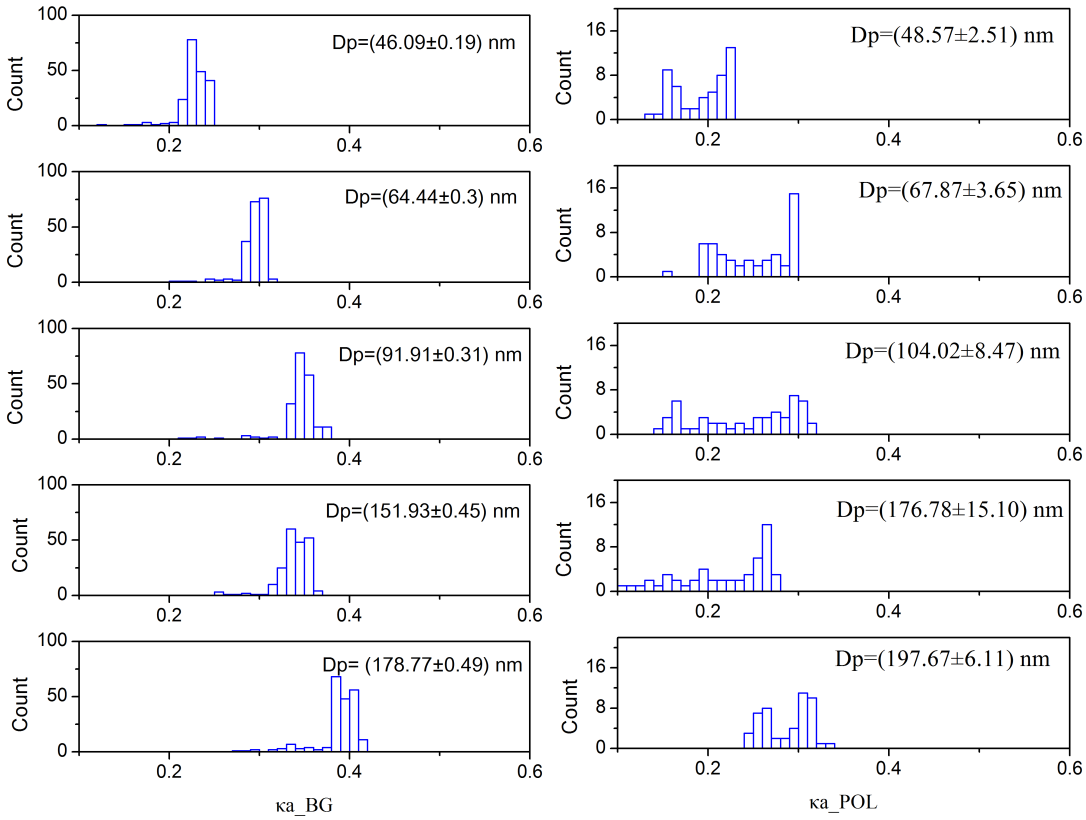

Fig. 4 PDF of κ_{cut} under background and polluted conditions at different particle size ranges during the size-resolved CCN measurements period.

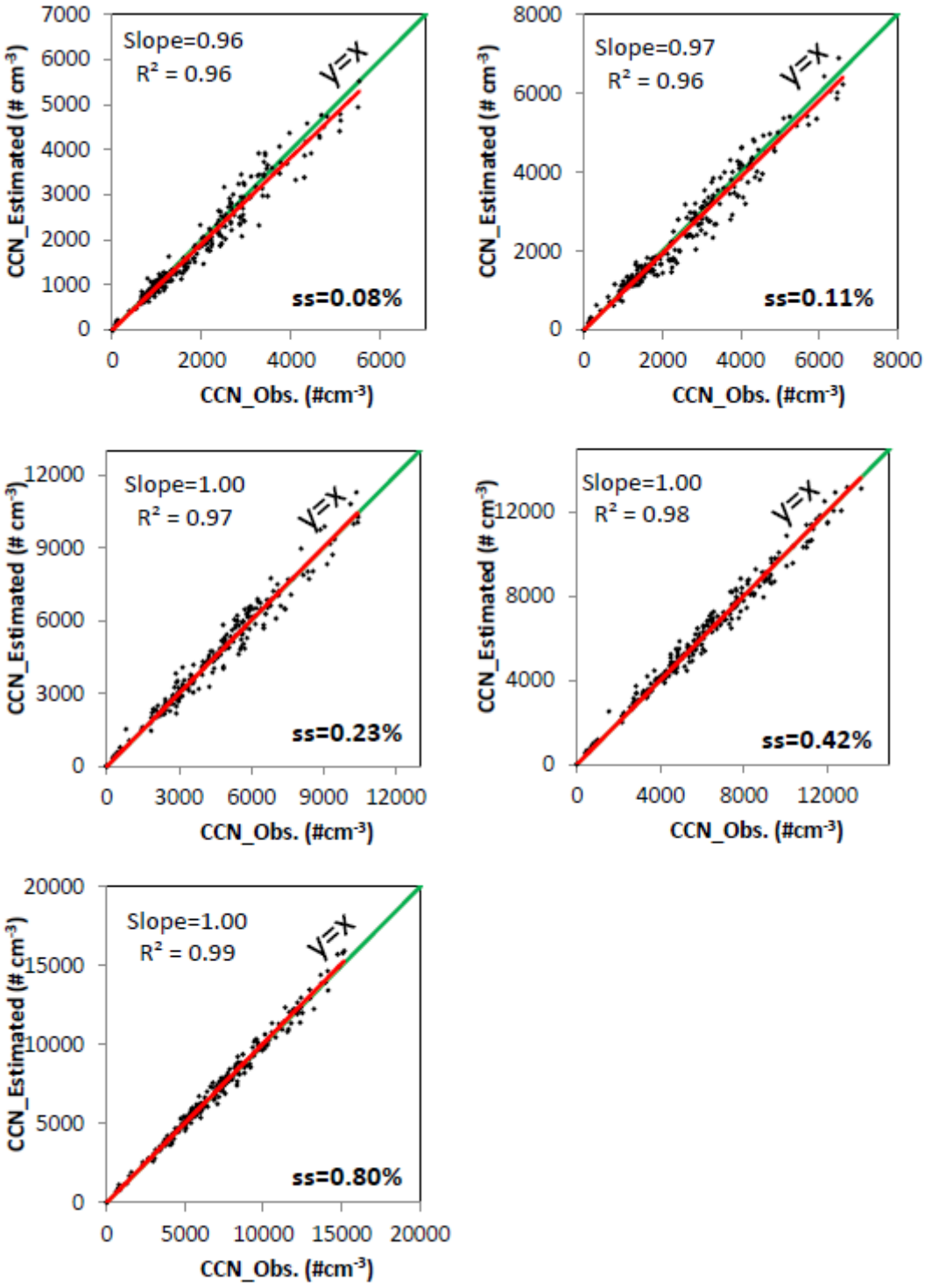

Fig. 5 Estimated N_{CCN} plotted against the observed N_{CCN} in parallel observation (PO) closure test. The green solid line is the 1:1 line.

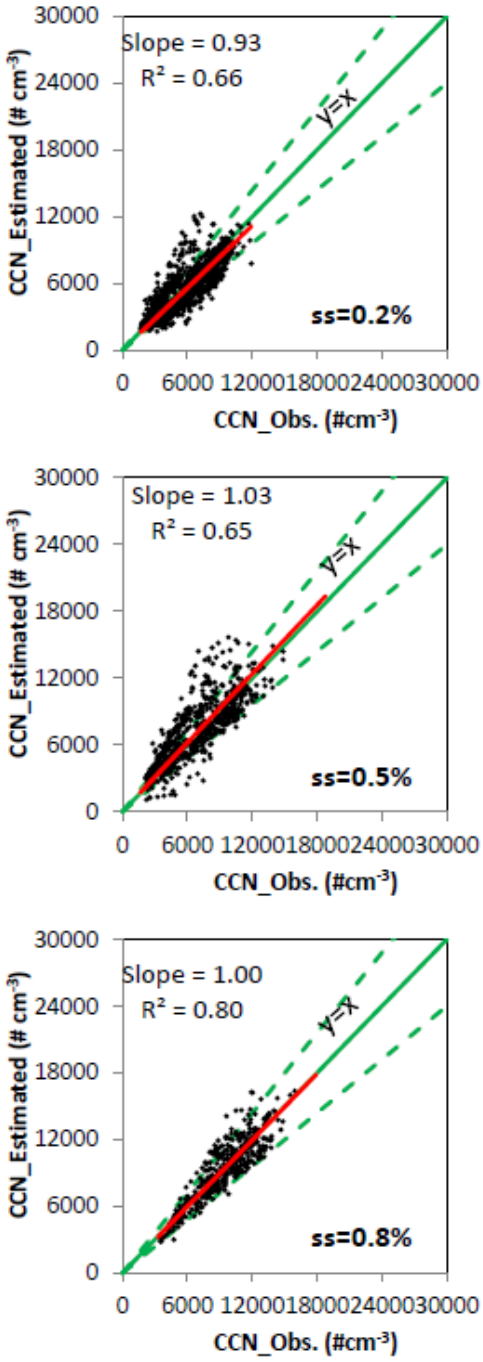

Fig. 6 Estimated N_{CCN} plotted against the observed N_{CCN} in Non-parallel observation (NPO) closure test. The green solid line is the 1:1 line, and the dashed green lines indicate the band of about ±30% deviation of N_{CCN}-estimated from N_{CCN}-observed.

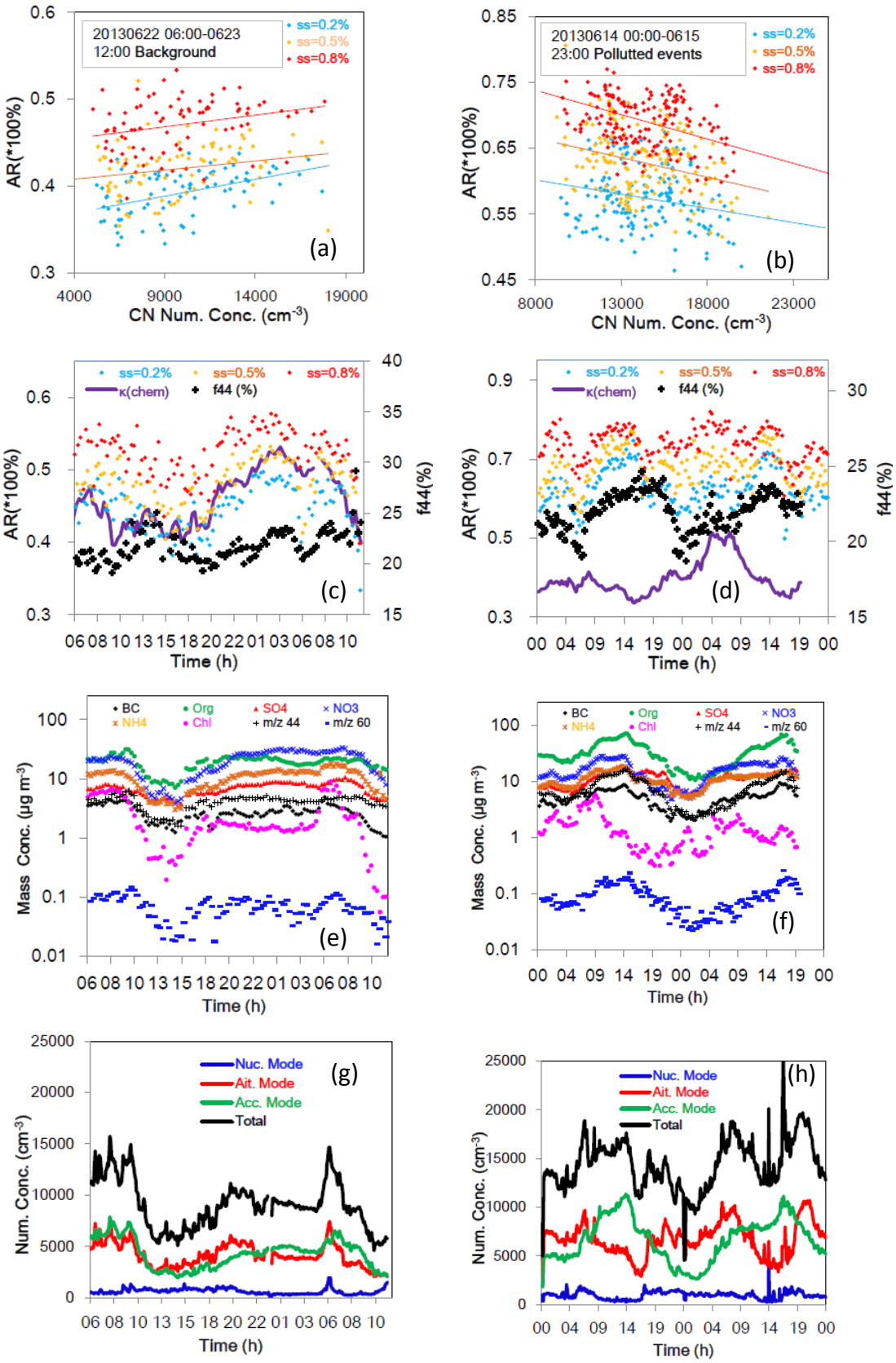

Fig. 7 Two selected cases of background conditions (22-23 June, 2013) with N_{CN} of <15000 cm^{-3} (left) and polluted events (14-15 June, 2013) with N_{CN} > 15000 cm^{-3} (right) during the campaign. Bulk CCN activation ratios (AR) at all three

supersaturations of 0.2%, 0.5% and 0.8% against N_{CN} in clear days and polluted days are shown in Fig 7a and Fig. 7b respectively. Diurnal variations of AR, derived κ_{chem} and fraction of total organic mass signal at *m/z* 44 (f44) are shown in Fig. 7c (background conditions) and Fig. 7d (polluted events). Mass concentrations of black carbon (BC), organics, nitrate (NO_3^-), ammonium (NH_4^+), sulfate (SO_4^{2-}), chloride (Cl^-) irons etc. are shown in Fig. 7e (background conditions) and Fig.7f (polluted events). N_{CN} at size range of nucleation, Aitken and accumulated mode are shown in Fig 7g and Fig. 7h for background conditions and polluted events respectively.

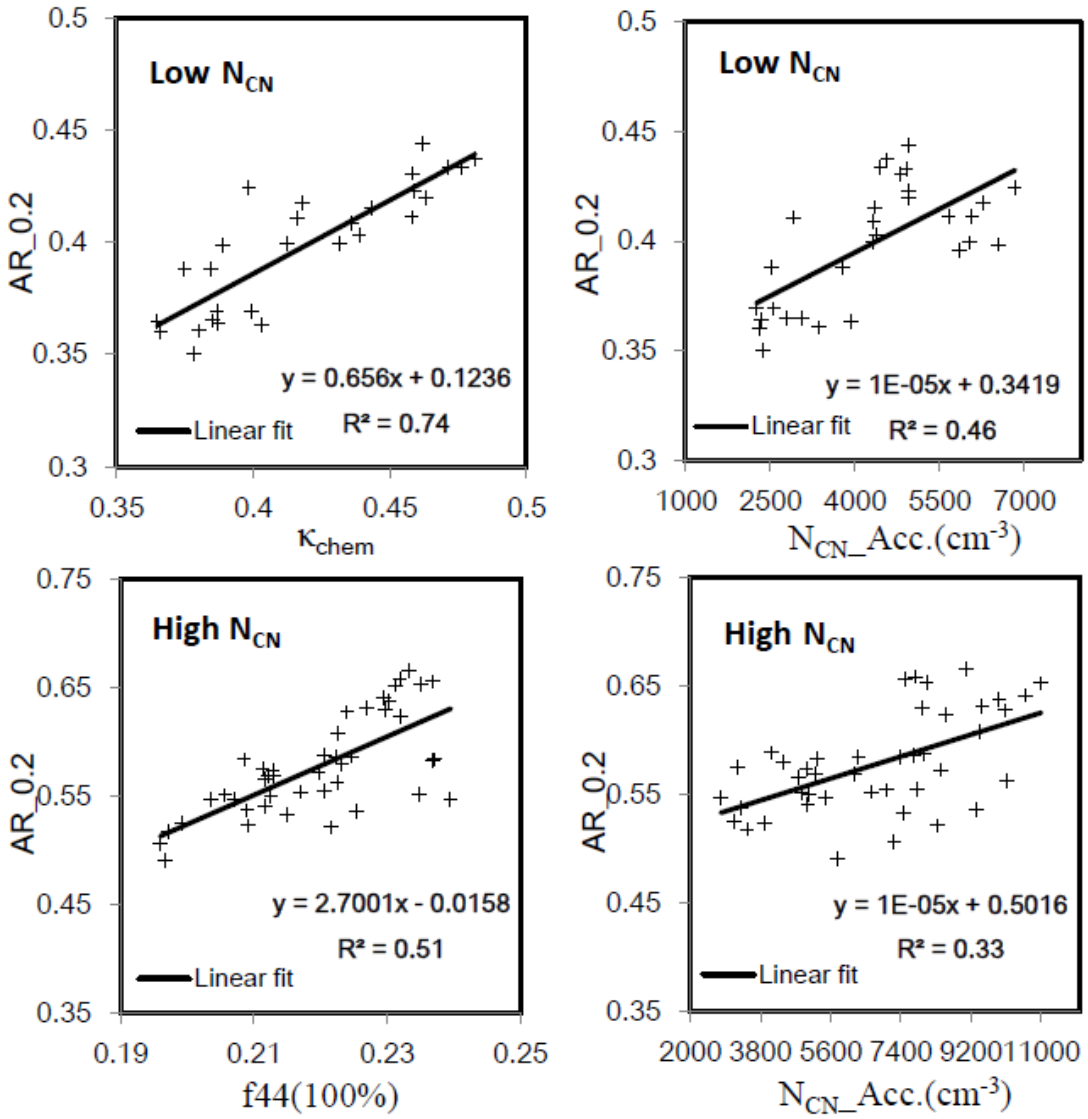

Fig. 8 Correlations of AR with κ_{chem}, *f*44 and N_{CN}_Acc. at background (with low N_{CN}) and polluted (with high N_{CN}) cases. The AR is measured at SS=0.2%, the N_{CN}_Acc. is CN number concentrations at accumulated modes.

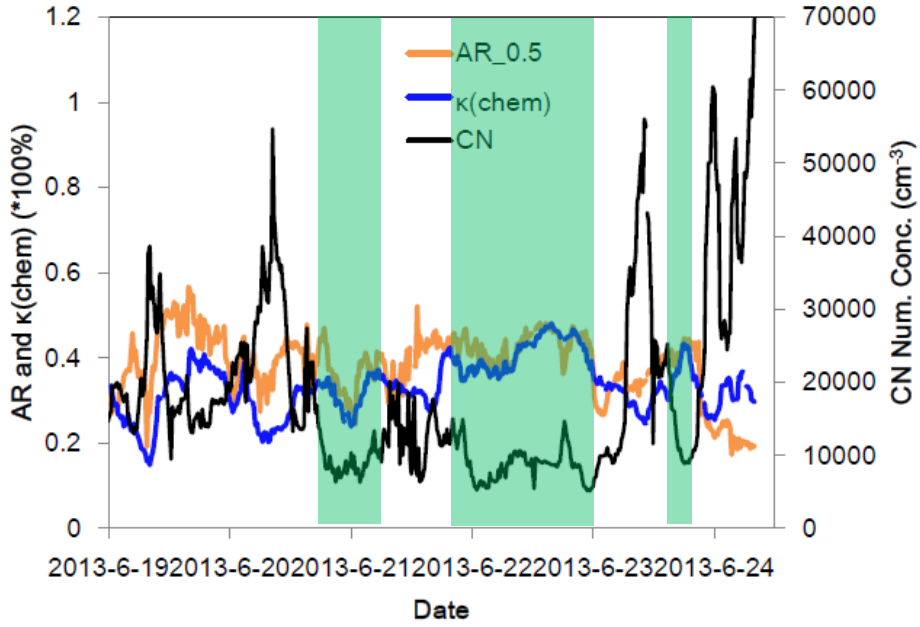

Fig. 9. An example for temporal variations of bulk AR at spersaturation of 0.5%, derived κ_{chem} and N_{CN} during the campaign (19-24 June, 2013). The periods (with low N_{CN}) when high correlations between bulk AR and κ_{chem} were observed were marked by rectangles in light green color.